JOURNAL OF GEOPHYSICAL RESEARCH, VOL. 87, NO. C8, PAGES 5731–5740, JULY 20, 1982

Analysis of Remotely Sensed Long-Period Wave Motions

G. A. MEADOWS[1]

Department of Atmospheric and Oceanic Science, University of Michigan, Ann Arbor, Michigan 48109

R. A. SHUCHMAN AND J. D. LYDEN

Radar and Optics Division, Environmental Research Institute of Michigan, Ann Arbor, Michigan 48107

Synthetic aperture radar has been used to image long-period (15–200 s) gravity waves in the nearshore region of Lake Michigan. These long-period waves are a response of the sea surface to forcing by a nonmonochromatic, wind-generated surface wave field. The synthetic aperture radar data were successfully compared with an in situ wave gauge record. Both one- and two-dimensional fast Fourier transforms were generated from near and offshore regions of synthetic aperture radar data. The synthetic aperture radar–derived near and offshore spectral estimates exhibited both low- and high-frequency wave components. Classical bathymetrically controlled wave refraction was observed for both the short as well as long wave components of the sea surface. This paper demonstrates the ability of X band synthetic aperture radar to detect low-amplitude, long-period signals. The signals appear to correspond to a 'surf beat' generated by the incident wind wave field.

INTRODUCTION

Since the initial observations of long-period (30–300 s) wave motions by *Munk* [1949] and *Tucker* [1950], several conjectures concerning the generation and propagation of 'surf beats' have been proposed. The theoretical development of *Longuet-Higgins and Stewart* [1962] employed interactions of a nonmonochromatic sea to generate an amplitude-modulated sea surface. Through the use of the calculated increased radiation stress beneath groups of large waves and a corresponding decrease in the stress associated with lower waves, a forced long-period wave is generated at the beat frequency. *Meadows* [1977] showed that this long-period forced wave propagated at the short wave group velocity and was observable in the nearshore zone. Similarly, *Larsen* [1979] has observed long-period forced waves in the North Pacific which appeared to have been generated by, and propagated with, the modulated sea surface.

All inferences, as well as previous attempts at field verification of the physical characteristics of these long-period waves, have been based on single point time series measurements. The studies of *Meadows* [1977] represented the first two-dimensional, synchronous time series observations of nearshore, long-period wave motions. These studies, however, were still conducted over an offshore spatial interval which was small (of the order of half the wavelength) compared to the wavelengths of the forced surf beat.

Investigation of the backscatter of microwave energy from the sea surface provides a unique way to view large spatial regions of the sea surface nearly simultaneously. Synoptic coverage of wave characteristics, as available from synthetic aperture radar (SAR), has provided a three-dimensional (two spatial dimensions and radar backscatter modulation) representation of the propagation and physical characteristics of long-period wave motions across the sea surface. Since the intensity of radar backscatter can be related to the characteristics of ocean wave propagation [*Gonzales et al.*, 1979; *Gower and Hughes*, 1979; *Shuchman and Meadows*, 1980; *Schwab et al.*, 1981], definitive information is now available concerning the generation and propagation of these wave motions.

SAR sea surface information was collected over a region of Lake Michigan by the Environmental Research Institute of Michigan (ERIM). At the time of the SAR overflight, the University of Michigan Department of Atmospheric and Oceanic Science was operating its mobile nearshore wave and current monitoring array [*Meadows*, 1979; *Meadows et al.*, 1980; *Shuchman and Meadows*, 1980]. The concurrent acquisition of airborne SAR sea surface data with in situ sea truth has provided a valuable opportunity to investigate the three-dimensional characteristics of a complex nearshore wave field. A previous paper, utilizing this coincident SAR and in situ wave gauge data [*Shuchman and Meadows*, 1980], has shown SAR can successfully image the incident wind-generated gravity wave field. This paper will concentrate on the long-period (15–200 s) response of the sea surface to forcing by a nonmonochromatic, wind-generated surface wave field and the ability of SAR to image successfully these subtle surface wave motions.

THEORY OF LONG-PERIOD WAVE GENERATION

Employing the classic formulation for the linear interaction of two sinusoidal waves of differing radian wave numbers k_1 and k_2 and radian wave frequencies σ_1 and σ_2, a solution for the resultant sea surface is possible by simple superposition of these wave components. The resultant sea surface η is a function of both space x and time t and is given by

$$\eta(x, t) = a \cos (k_1x - \sigma_1t) + a \cos (k_2x - \sigma_2t) \qquad (1)$$

where a is the wave amplitude. As suggested by *Kinsman* [1965] for the condition when the two component waves are very nearly the same length and period, such that

$$\Delta k \ll k_1 \qquad \Delta\sigma \ll \sigma_1$$

[1] Also a consultant at Environmental Research Institute of Michigan, Ann Arbor, Michigan 48107.

Paper number 2C0261.
0148-0227/82/002C-0261$05.00

where $\Delta k = k_1 - k_2$ and $\Delta\sigma = \sigma_1 - \sigma_2$, then

$$k_1 \approx k_2 \qquad \sigma_1 \approx \sigma_2$$

Hence the amplitude-modulated sea surface, as a function of distance in the propagation direction, may be expressed as

$$\eta(x) \approx 2a \cos\left(\frac{\Delta k}{2} x\right) \cos(kx) \tag{2}$$

and as a function of time as

$$\eta(t) \approx 2a \cos\left(\frac{\Delta\sigma}{2} t\right) \cos(\sigma t) \tag{3}$$

Since $\Delta k \ll k$ and $\Delta\sigma \ll \sigma$, the spatial and temporal scales of the modulation are very long compared to the individual wave components which comprise the group. This interference pattern results in the generation of groups of large waves separated by groups of small waves (see Figure 1 from *Longuet-Higgins and Stewart* [1962]). The length of the long-period modulation is given by *Kinsman* [1965] as

$$L_{\text{mod}} = \frac{4\pi}{\Delta k} \tag{4}$$

while the period of the modulation is

$$T_{\text{mod}} = \frac{4\pi}{\Delta\sigma} \tag{5}$$

The distance between successive groups of high waves is therefore $\frac{1}{2} L_{\text{mod}}$, and the corresponding time interval is $\frac{1}{2} T_{\text{mod}}$.

Consider a conventional right-handed rectangular coordinate system with the x axis horizontal and in the direction of wave propagation and the z axis vertical and upward. Let u, v, and w be the velocity components in the x, y, and z directions, respectively, and let p, ρ, and g denote the pressure, density, and gravitational acceleration, respectively. Also, let the free surface be given by the equation $z = \eta(x, y, t)$, where t is time, and the rigid horizontal bottom by the equation $z = -h$.

When the length of the modulated wave groups are long compared to the local water depth, changes in the mean sea level and the wave mass-transport correspond to those that would result from an applied horizontal force, in this case the radiation stress [*Whitham*, 1962; *Longuet-Higgins and Stewart*, 1962]. For this condition, the flux of momentum across an x = constant vertical plane is given by *Longuet-Higgins and Stewart* [1962] as

$$S = \overline{\int_{-h}^{\eta} (p + \rho u^2) dz} \tag{6}$$

where the radiation stress S_x is the difference between S and the contribution due to the hydrostatic pressure;

$$S_x = \overline{\int_{-h}^{\eta} (p + \rho u^2) dz} - \int_{-h}^{\bar\eta} \rho g(\bar\eta - z) dz$$
$$= S - \tfrac{1}{2}\rho g(h + \bar\eta)^2$$

which is approximately equal to

$$\approx S - \rho g(\tfrac{1}{2} h^2 + h\bar\eta) \tag{7}$$

where the overbars denote time averages. For the condition of long waves in shallow water, the vertical accelerations are assumed negligible, hence, correct to second order

$$S_x = E\left[\frac{2C_g}{C} - \frac{1}{2}\right] \tag{8}$$

where E is the wave energy per unit horizontal area and is defined as

$$E = \tfrac{1}{2} \rho g a^2$$

C_g in (8) denotes the deep water group velocity of the waves, and C is the phase speed of the individual waves.

Conservation of mass and momentum may be expressed as

$$\frac{\partial(\rho\bar\eta)}{\partial t} + \frac{\partial M}{\partial x} = 0 \tag{9}$$

and

$$\frac{\partial M}{\partial t} + \frac{\partial S}{\partial x} = 0 \tag{10}$$

where M is the mean, vertically integrated horizontal momentum given by

$$M = \overline{\int_{-h}^{\eta} \rho u dz} \tag{11}$$

Substituting for S_x from (7), the momentum equation may be written as

$$\frac{\partial M}{\partial t} + gh \frac{\partial}{\partial x} (\rho\bar\eta) = -\frac{\partial S_x}{\partial x} \tag{12}$$

Since the applied force $-\partial S_x/\partial x$ travels with the group velocity, $\partial/\partial t$ may be replaced with $-C_g\partial/\partial x$, which upon substitution into (9) and (12) gives

$$-\rho C_g \frac{\partial\bar\eta}{\partial x} + \frac{\partial M}{\partial x} = 0 \tag{13}$$

and

$$\rho gh \frac{\partial\bar\eta}{\partial x} - C_g \frac{\partial M}{\partial x} = -\frac{\partial S_x}{\partial x} \tag{14}$$

The solution to this set of equations is given by *Longuet-Higgins and Stewart* [1962] as

$$\rho \frac{\partial\bar\eta}{\partial x} = -\left(\frac{1}{gh - C_g^2}\right) \frac{\partial S_x}{\partial x} \tag{15}$$

and

$$\frac{\partial M}{\partial x} = -\left(\frac{C_g}{gh - C_g^2}\right) \frac{\partial S_x}{\partial x} \tag{16}$$

Upon integration, the free surface elevation and mean horizontal momentum become

$$\bar\eta = -\frac{S_x}{\rho(gh - C_g^2)} \tag{17}$$

and

$$M = -\frac{C_g S_x}{(gh - C_g^2)} \tag{18}$$

respectively.

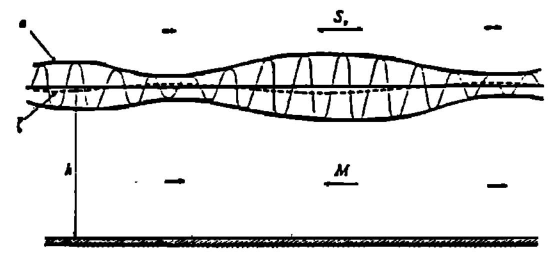

Fig. 1. Schematic representation of the forced long-period modulation of the surface resulting from short wind-generated wave component interactions [from *Longuet-Higgins and Stewart*, 1962]

The interpretation suggested by *Longuet-Higgins and Stewart* [1962] is as follows:

> It will be noticed that beneath a group of high waves, where S_x and E are both large, $\bar{\eta}$ and $\bar{u}$ are more negative, that is to say there is a relative depression in the mean surface level, coupled with a mean flow opposite to the direction of wave propagation. Beneath a group of low waves, on the other hand, the mean surface level is raised and the flow is positive.

(See Figure 1.)

SEA SURFACE-SAR INTERACTIONS

It is generally accepted that the scattering of microwave energy from the sea surface is a Bragg-Rice resonance phenomenon [*Wright*, 1968], thus making the received radar image particularly sensitive to capillary and short ultragravity ocean surface waves. Nonlinear interaction of these short waves with longer period wave motions is the subject of much research [*Phillips*, 1981; *Longuett-Higgins and Stewart*, 1964; *McGoldrick*, 1970, 1972]. It is generally agreed, however, that the short wavelengths are increased in the troughs of the long waves and that the correspondingly short wave height is decreased. Conversely, on the wave crest of the long waves, the short wave height is increased and the short wavelength is decreased. Both effects act to increase the sea surface roughness in the crest regions of long waves and correspondingly decrease the roughness in the trough region [*Phillips*, 1981]. The radar backscatter increases as a function of increasing sea surface roughness, thus producing regions of intense radar backscatter from modulated long wave crests and diminished radar return from modulated long wave troughs. Furthermore, it also appears that the existence of a surface capillary or ultragravity wave field is a necessary condition to provide radar images of long-period ocean internal wave motions.

The proposed physical mechanism for the indirect imaging of 'surf beats' by radar backscatter is as follows. A modulated, wind-driven, capillary/ultragravity wave field exists in conjunction with a shoreward propagating, nonmonochromatic, gravity wave field. Nonlinear capillary-gravity wave interactions occur which produce increased surface roughness on the crests of the gravity waves and decreased surface roughness in the troughs. Concurrently, similar but slightly different gravity wave components of the nonmonochromatic wave field are interacting to form surf beats consisting of groups of high waves separated by groups of low waves. These wave groups produce corresponding depressions and relaxations of the mean water level in response to fluctuations of the applied radiation stress. Hence a forced, long-period wave, traveling at the group velocity of the wind wave packet, is generated. Bright radar returns, therefore, should correspond to groups of high-gravity waves and corresponding troughs of the forced long-period waves.

DATA DESCRIPTION

The synthetic aperture radar (SAR) used to collect the data is the ERIM X and L band dual polarized radar described by *Rawson et al.* [1975]. The ERIM SAR system records four channels of radar return, but we will focus our attention here on the X band horizontal-transmit-horizontal-receive (HH) channel, as this data provided the clearest wave images. The SAR was flown at an altitude of 6100 m and operated with a center incident angle from the vertical of 20°, yielding a swath width of 5.6 km. The cross-track or range resolution of SAR is limited by radar bandwidth and is about 2 m for X band. The along-track or azimuth resolution is obtained from the synthetic aperture technique described by *Brown and Porcello* [1968]. For the X band, the azimuthal resolution is about 2.5 m. This SAR data was processed on the ERIM tilted-plane precision optical processor described by *Kozma et al.* [1972].

The SAR data was collected on October 18, 1978, at approximately 1635 EST. The airborne data was collected along the shoreline of Lake Michigan centered at latitude 43°50′ N. The site for this field experiment as shown in Figure 2 was the eastern shore of Lake Michigan, between the cities of Ludington and Pentwater, Michigan. This thirteen kilometer section of shoreline, extending approximately north-south, is characterized by a multiple-barred bathymetry with nearly straight and parallel contours.

At the same time as the ERIM flight, the University of Michigan Department of Atmospheric and Oceanic Science was operating its mobile surf zone, wave, and current sensing array [*Meadows*, 1979]. Monitoring of incident wave characteristics and longshore current velocities was conducted through the growth of a major storm on Lake Michigan. A detailed discussion of the experimental design is presented by *Wood and Meadows* [1975] and *Meadows* [1977]. Surface-piercing, step-resistance wave probes and bidirectional ducted impeller flow meters were used to make simultaneous measurements of wave and current conditions. These sensors were oriented on a line perpendicular to

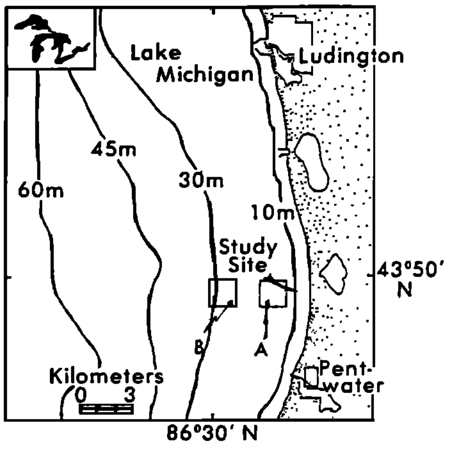

Fig. 2. General study area showing nearshore bathymetry and location of fast Fourier transformed SAR data.

shore, extending from the beach to the outer surf zone. Other coastal sensing equipment included a directionally mounted motion picture camera and Lagrangian drifters. Unfortunately, high wind and wave action on October 17 and 18 destroyed much of the array; however, sufficient sensors survived to make this comparative study possible.

METHODS

The SAR collected data were digitized with an approximate resolution of 6 m (3-m pixels) by using the ERIM hybrid image dissector [*Ausherman,* 1975]. The range coordinates of the digitized data were analytically corrected for slant-to-ground range geometry [*Feldkamp,* 1978]. Two 1.5 × 1.5 km subsections (see Figure 2) with 6-m resolution were extracted from the digitized data. The two sections are labeled A and B, where A is closest to shore.

The 3.0-m pixel digitized SAR images were converted to 6-m samples by 4 pixel into 2 pixel averaging in order to decrease the speckle in the image. The average value of each azimuthal line was subtracted from the line to remove the trend of intensity falloff with increasing range distance. Two-dimensional fast Fourier transforms (FFT's) were performed on each 256 × 256 cell subsection to yield raw directional wave number spectra with a Nyquist wave number of 0.5 m^{-1}. The raw spectra were smoothed by replacing each value with the average of the surrounding 5 × 5 cell. The approximate number of degrees of freedom for the resulting spectrum is 142 [*Kinsman,* 1965]. The 99% confidence limits are then ±1.5 dB [*Jenkins and Watts,* 1968].

In addition to the two-dimensional FFT analysis, five isorange SAR backscatter records 1.5 km long were analyzed by using both a one-dimensional spectral analysis and a band pass filtering program. This one-dimensional analysis was performed on the SAR data to better quantify the long-period components of the prevalent wave field. To perform this analysis, five adjacent isorange lines of data were extracted from the digital image corresponding to the center of both study areas A and B. These lines were then averaged or, in effect, smoothed in the range direction; this was done to reduce the speckled nature of the SAR data. The averaged lines were then plotted in order to characterize the relative backscatter across these study areas. These data were then selectively filtered for wavelengths between 177 and 1180 m for study area A and from 249 to 1660 m for study area B. This wavelength filtering corresponds to the temporal region of interest, 15–200 s.

To calculate the directional wave spectrum at the instrumented surf zone site, a 16-min analog record was digitized at 0.25-s intervals and analyzed by using conventional one-dimensional fast Fourier transform techniques. The directional information was obtained from the directionally mounted camera. One-dimensional spectral analysis using a FFT routine was performed on the total 16-min, outer surf zone water level elevation time history. The smoothed spectrum resulting from this analysis is presented in Figure 3. This spectrum exhibits a well-defined broad peak in the wind wave range (2–8 s), composed of multiple components. This spectrum is characteristic of locally generated seas. In addition, this spectral analysis has also identified significant long-period wave motion at specific periods of 17.2 and 32.3 s and a less significant peak at approximately 59 s. These nearshore spectral estimates were obtained from a continuous digital record consisting of 3840 equally spaced values at 0.25-s intervals. The 80% confidence band lies between 1.42 and 0.62 times the spectral estimate and is indicated on Figure 3 [*Kinsman,* 1965].

Based upon these results, this total water level elevation record was band pass filtered to retain only surface wave motions with periods between 15 and 200 s. A representative portion of the original and band pass filtered, long-period records is presented in Figure 4. It, therefore, appears that significant long-period wave motions are present in the nearshore region with a mean amplitude of approximately 10% of that of the incident wind waves. These results agree favorably with the finding of *Meadows and Wood* [1982] where both progressive as well as standing long-period wave motions were observed in the nearshore region. The question arises, however, as to the generation mechanism of these waves. It is the hypothesis of the authors that these long-period waves are formed as a result of nonlinear interactions between the dominant wind-wave components and that they propagate as forced waves at the group velocity of wind-generated waves. Hence it should be anticipated that these wave motions should exist somewhat homogeneously across the sea surface provided that wind waves of sufficient amplitude and prescribed frequency exist.

ANALYSIS

Synthetic aperture radar provides a unique perspective from which to investigate this hypothesis, namely, that long-period surf beats are generated by and propagate with the wind wave field. The nearly simultaneous view of a relatively large spatial region of the sea surface provided by either an airborne or spaceborne SAR affords an ideal measurement tool for these wave motions. To examine this capability, the results of both the SAR two-dimensional and the nearshore in situ wave gauge data series will be evaluated.

Results of the nearshore step resistance wave gauge spectral analysis have indicated several well-defined peaks in the wind wave range. In addition, two long-period peaks at 17.2 and 32.3 s, respectively, were also well resolved. A poorly resolved spectral peak is also apparent at approximately 59 s. Linear combinations of the dominant wind wave components are formed in Table 1 to produce their respective beat periods. It may be noted that the dominant wind wave components of 5.6, 4.8, and 4.2 s combine, theoretically, to form beats of 16.8 and 33.6 s, respectively. These calculated beat periods are very close to those periods resolved by the spectral analysis of the total 16-min water

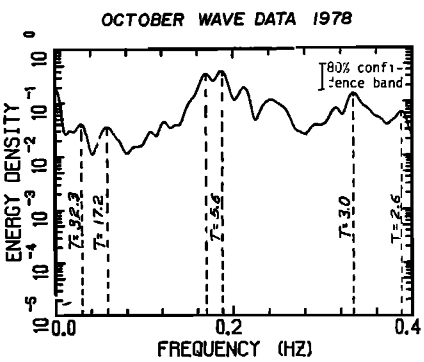

Fig. 3. One-dimensional wave height spectrum of water surface elevation time history from resistance wave gauge. Dominant wave periods are identified.

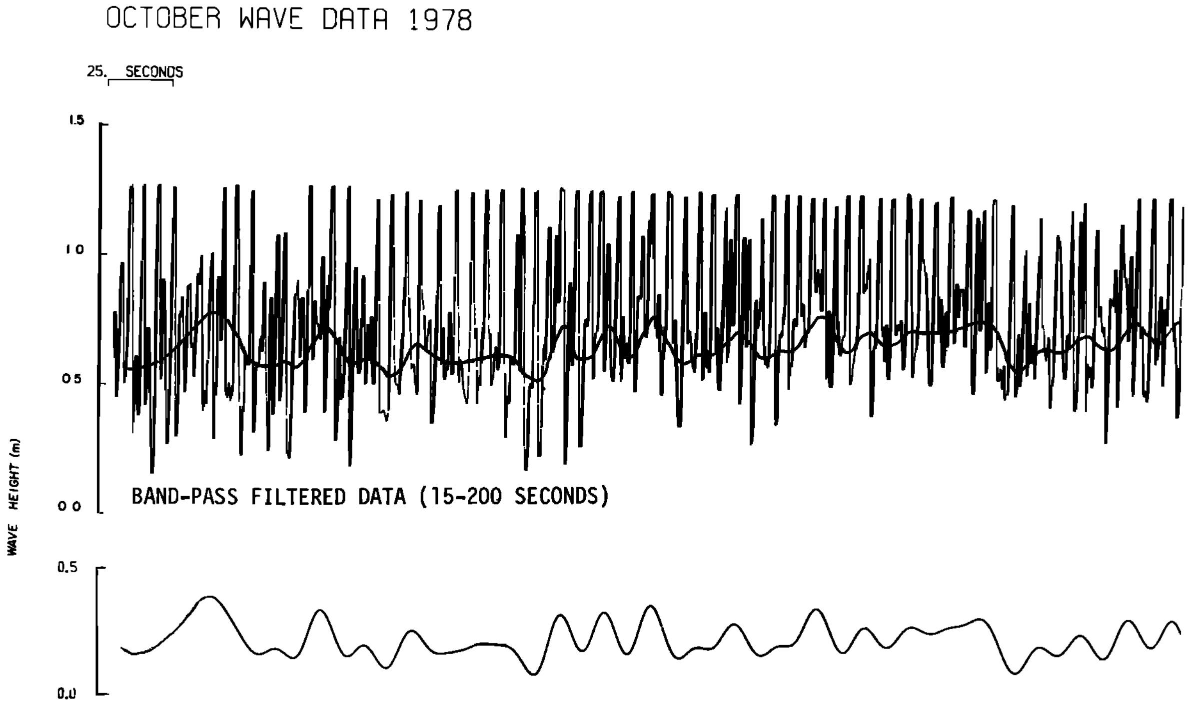

Fig. 4. Representative section of 16-min time history of water elevation data from resistance wave gauge. Also shown is the corresponding 15–200 s band pass filtered data. (Note the negative correlation [180° phase shift] between the wind wave amplitudes and the mean surface level.)

surface elevation recorded from the nearshore wave gauge. It therefore appears that forced long-period wave motions were present in the nearshore region resulting from the nonlinear interaction of the dominant wind wave components.

The energy associated with these long-period forced waves is an order of magnitude below that of the peak in the wind wave spectra. Theoretical calculations of the maximum mean surface deformation from (17) suggest a forced wave height of approximately 0.38 m. The energy associated with the forced wave would be approximately a factor of 8.4 less than that associated with the peak wind wave component. It appears that long-period wave motion in the nearshore region is present with both a period and an amplitude close to theoretical predictions.

To further identify these long-period wave motions, the total 16-min water surface elevation record from the nearshore wave gauge was band pass filtered for periods between 15 and 200 s. A representative portion of the original water surface elevation record and its associated long-period component are presented in Figure 4. This series, as well as the data of *Meadows* [1977], suggests that the mean surface level

TABLE 1. Calculated Beat Periods

Input Components, s	Input Components, s				
	5.6	4.8	4.2	3.0	2.6
5.6	...	33.6	16.8	6.5	4.9
4.8	...	...	33.6	8.0	5.7
4.2	...	...	...	10.5	6.8
3.0	...	...	...	...	19.5
2.6	...	...	...	...	...

is 180° out of phase with the wind wave amplitudes. As theoretically suggested, this implies that depressions in the water surface are associated with groups of large waves and long-period elevations of the water surface correspond to groups of low waves.

Based upon these considerations, SAR imagery of a relatively large region of the sea surface should also exhibit these long-wave features. In an effort to investigate this potential of SAR, a manual photo-interpretation of the radar image film was performed. A portion of the *X* band (HH) SAR data collected over the Lake Michigan test site is presented in Figure 5. The image extends 7.9 km offshore and is 5.6 km wide. Alternating groups of large and small wind wave packets can be readily seen across this image. At three representative locations across this nearshore imagery, the long-wave lengths are indicated on the figure. As these long waves, forced by short-wave groups, propagate shoreward, both wavelength compression and refraction are plainly observable. The long wavelengths decrease from approximately 510 m (area B) to approximately 410 m (area A). These radar observations of the long wave components of surface elevation are in excellent agreement with sea truth measurements made at the outer surf zone.

To further document the existence and propagation characteristics of these SAR-sensed long wave components, a conventional two-dimensional FFT of the radar backscattered energy was performed. One FFT analysis was performed in both the offshore and nearshore regions of the aircraft swath. The SAR FFT's were generated by the algorithm described by *Shuchman et al.* [1979]. However, in this application, only the long-wave portion of the spectrum is of interest. For a detailed discussion of the total SAR-sensed wave spectra and associated sea truth see *Shuchman and Meadows* [1980]. A summary of the general sea state

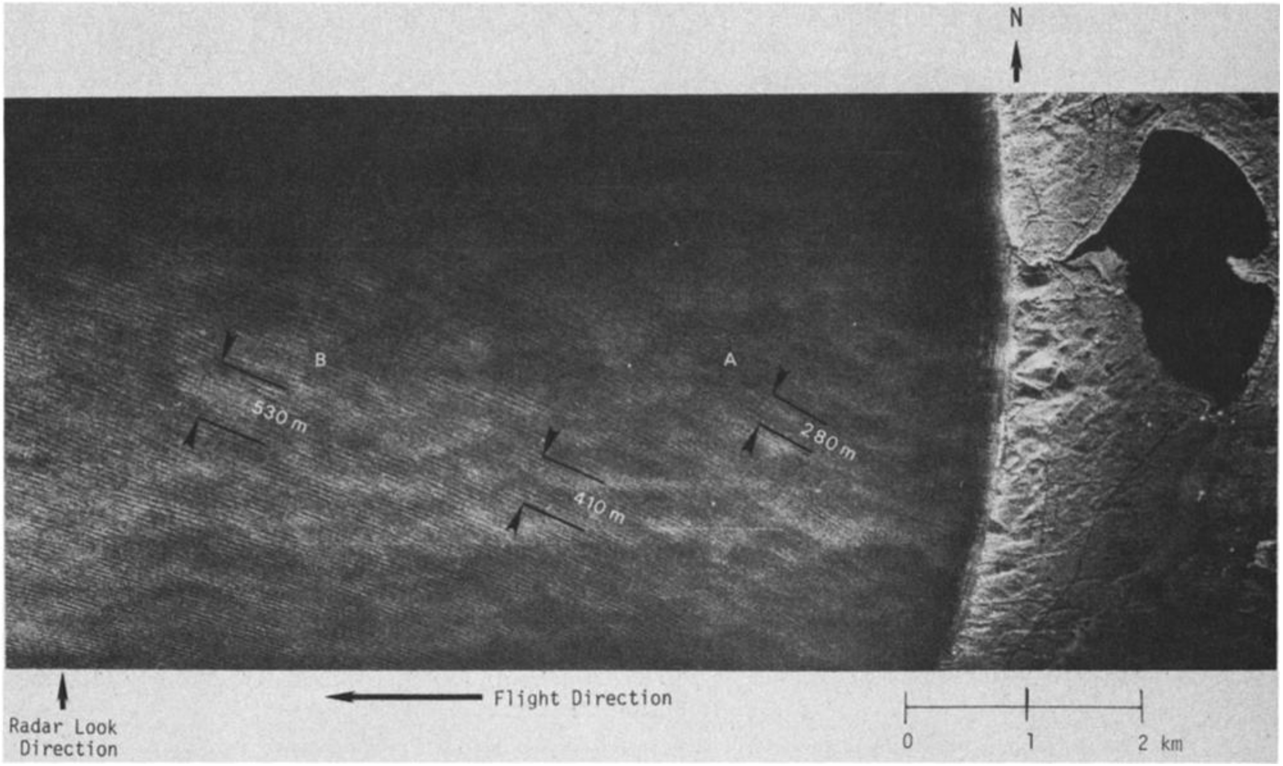

Fig. 5. *X* band (HH) SAR image of test site showing long-period wave components.

conditions during this experiment as well as a comparison of the SAR-derived, wind-generated sea spectral estimates to sea truth are presented in Table 2.

In the offshore region, the SAR-derived spectral analysis resolved a long-wave component with energy concentrated at a wavelength of approximately 511 m, traveling in a direction of 025 ± 3°T. Similarly, in the nearshore region, a long-wave component of 408 m wavelength traveling at 035 ± 3°T was resolved. The nearshore and offshore two-dimensional FFT's are shown in Figures 6 and 7, respectively. Also shown on each of the figures is the one-dimensional plot of the low-frequency components versus relative energy. These estimates of long-wave characteristics exhibit two important properties. First, the long wavelengths are in excellent agreement with the representative offshore wave group dimensions derived from the SAR image film. Second, the degree of observed refraction from the offshore to the nearshore region of these forced long-period wave motions is also in close agreement with the sea truth as well as with the calculated wave refraction for the dominant wind wave components. A comparison of SAR-derived and sea truth wave characteristics is presented in Table 3.

Furthermore, the two directly observed quantities which determine the propagation of these SAR and sea truth sensed long-period wave motions are the length and period of the modulated wave group. The lengths of the dominant long-

TABLE 2. Comparison Between the SAR-Derived Surf Zone Conditions and the in Situ Sea Truth

		SAR-Derived Estimates		Sea Truth*	
Distance From Shore, m	Depth, m	Dominant Short-Period Wavelengths, m	Direction, T°	Dominant Short-Period Wavelengths, m	Direction, T°
900	10.5	48	35 ± 3	48	34 ± 2
		43		44	
2200	14.0	55	30 ± 3	54	30 ± 2
				44	
4600	27.0	55	25 ± 3	55	28 ± 2
		43		46	
		48			
6900	31.0	55	25 ± 3	55	28 ± 2
		48		46	

*Actual measurements made at surf zone; values for test areas are depth-corrected [*Shuchman and Meadows*, 1980].

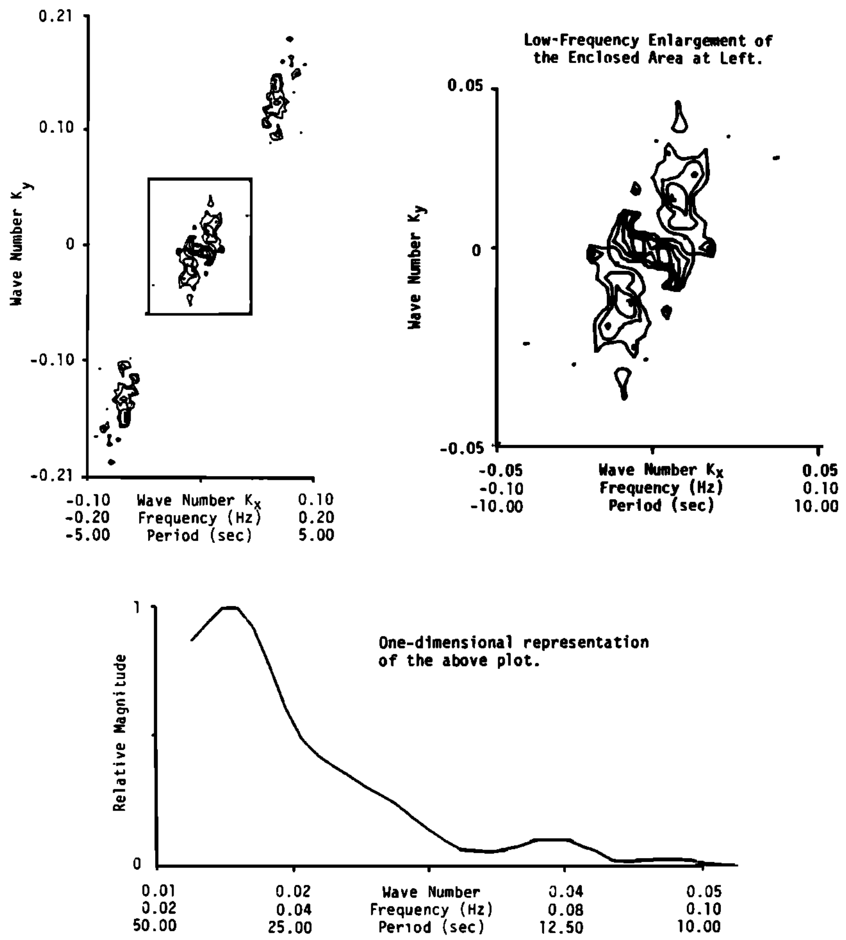

Fig. 6. SAR-derived two-dimensional spectral estimate (nearshore). (Note: Negative wave numbers, frequencies, and periods are included due to the symmetric nature of a two-dimensional FFT. The frequency and period axes assume shallow water waves; see text for further explanation.)

period waves were obtained from the SAR-derived, two-dimensional FFT. Similarly, the periods of the dominant long-wave components were obtained from a one-dimensional spectral analysis of the nearshore wave gauge data. By combining equations (4) and (5), the celerity of these modulated long-period waves may be expressed as

$$C_{\text{mod}} = \frac{L_{\text{mod}}}{T_{\text{mod}}} \tag{19}$$

The calculated long-period wave celerity utilizing both the SAR and wave gauge measured dominant long-period wave parameters, results in values of 12.6 ms^{-1} and 15.8 ms^{-1} for areas A and B, respectively. It is interesting to note that assuming these long-period waves are propagating as shallow water waves with celerity given by

$$C = \sqrt{gd} \tag{20}$$

long-period wave celerities of 12.6 ms^{-1} and 16.8 ms^{-1} are calculated for areas A and B, respectively. On the basis of this close agreement, it appears that these observed long-

TABLE 3. Comparison Between the Long-Period SAR-Derived Spectral Estimates and the in Situ Sea Truth

			SAR-Derived Estimates		Sea Truth*	
Test Area	Distance From Shore, m	Depth, m	Dominant Long-Period Wavelengths, m	Direction, T°	Dominant Long-Period Wavelengths, m	Direction, T°
A (Nearshore)	2650	16.2	157–167	35 ± 3	216	34 ± 2
			393–423		406	
B (Offshore)	5800	28.7	498–523	25 ± 3	288	28 ± 2
					541	

*Actual measurements made at the surf zone; values for test areas A and B are depth-corrected.

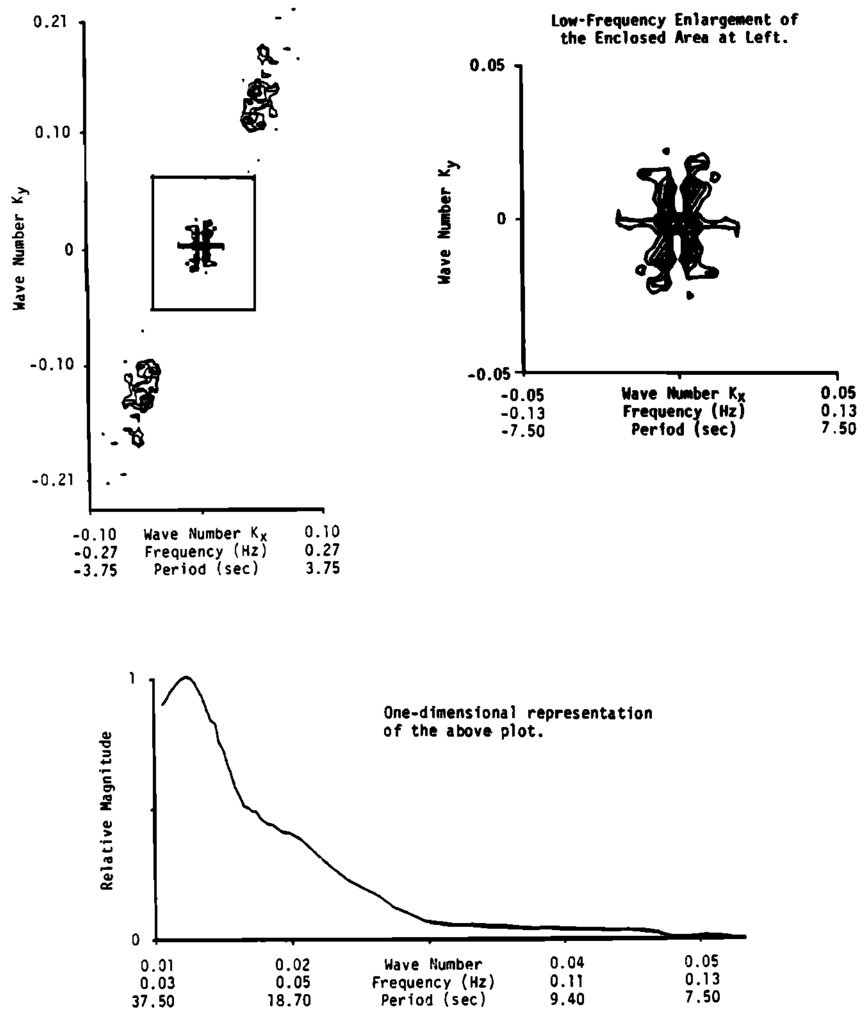

Fig. 7. SAR-derived two-dimensional spectral estimate (offshore). (Note: Negative wave numbers, frequencies, and periods are included due to the symmetric nature of a two-dimensional FFT. The frequency and period axes assume shallow water waves; see text for further explanation.)

period wave motions are propagating as shallow water waves and not as forced waves as suggested from theory. This apparent discrepancy arises from a complex interaction between the relatively short, steep, locally generated waves and the shallow bathymetry of this region. The theoretical formulation employed in this study is based upon the assumption that the character of the SAR-sensed modulated sea surface is a function of ΔK of the wind wave components, and that $\Delta K \ll K_1$. Hence, for limited fetch situations such as the conditions of this study, the two wind wave components separated by ΔK do not explicitly satisfy the mathematical constraint of $\Delta K \ll K_1$. This produces a modulated long-period wave which is not completely 'phase locked' with the short wave components and, in fact, appears to propagate as a shallow water wave.

The close agreement between the long-period celerity derived above and that predicted for a shallow water wave prompted the inclusion of frequency and period axes on the various plots in Figures 6 and 7. Recall that the SAR only provides a spatial measure of waves, therefore, the only 'true' axes in Figures 6 and 7 is that for wave number. The frequency and period axes are both based on the shallow water wave assumption for a given wave number. They are not derived from any physical measurements.

To document further the existence and character of the SAR-sensed long-period wave motions, one-dimensional scans of the raw radar backscatter were obtained. One spatial series, consisting of 512 digital values sampled at 3 m, was obtained from each of the two regions where the two-dimensional FFT analysis was performed. Area A was centered 2650 m offshore and area B was centered at 5800 m offshore. The total series of radar backscatter as well as their associated band pass filtered (177–1180 m, area A and 249–1660 m, area B) long-period components are presented in Figure 8. Once again, long-period oscillations of the radar backscatter intensity are clearly visible, with maximum radar return occurring in phase with peaks of the long-period oscillations (i.e., groups of large wind waves). These SAR-sensed, long-period oscillations represent approximately a 1.5-dB change in radar backscatter intensity from crest to trough. The dynamic range of the total, unfiltered radar backscatter intensity is approximately 5.2 dB. Hence the energy associated with these radar-sensed long-period oscillations is approximately a factor of 2.3 less than the energy of the radar backscatter associated with the wind wave components of the sea surface structure.

SUMMARY

It appears that a direct correlation exists between the amplitude of these long-period wave motions, as sensed in

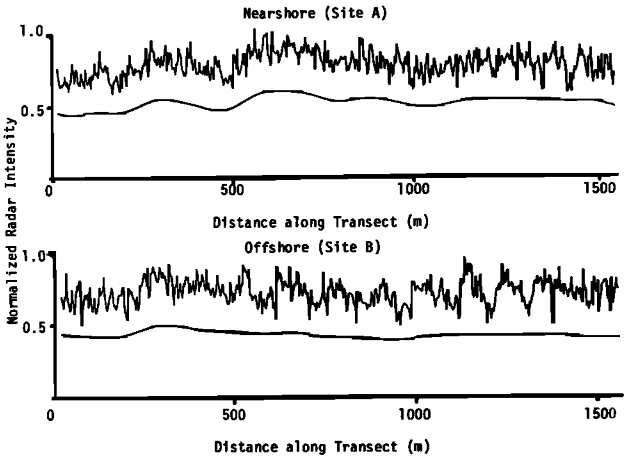

Fig. 8. Filtered and unfiltered radar transects for both near and offshore study sites.

situ, and the long-period component of the radar backscatter. From the sea truth measurements, the ratio of short-period wave to long-period wave mean amplitude is 5.4. Similarly, for the radar-sensed long-period oscillation this ratio is approximately 6.0. *Kasischke* [1980] has reported a linear relationship between SEASAT SAR modulation depth (crest-to-trough intensity) and wave height.

Investigation of the information contained in the backscatter of microwave energy from the sea surface can provide detailed and nearly synoptic coverage of relatively large portions of the ocean surface. To illustrate this unique capability, a three-dimensional representation of a portion of a SAR-sensed sea surface is presented in Figure 9, which depicts the long-period undulations present in study area B. This plot was produced from the SAR digital data by extracting six isorange lines of 5 pixels each, averaging these 5 pixels, in effect, to smooth in the range direction. These lines were then band pass filtered for wavelengths between 249 and 1660 m (15–200 s), and this filtered output was used as input to a perspective view-plotting program.

It is clear from this plot that long-period waves are present in this area. However, care should be exercised in interpreting what information this plot contains. This is merely a convenient graphical technique that shows the long-period components, not a detailed analysis technique.

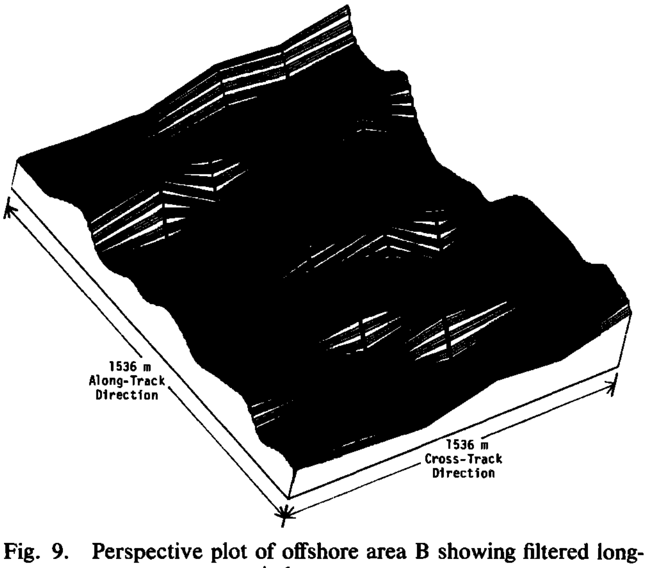

Fig. 9. Perspective plot of offshore area B showing filtered long-period components.

This paper has demonstrated that a synoptic remote sensing device such as SAR has the ability to successfully image low-amplitude, long-period signals (surf beats). The analysis techniques utilized to extract this information from the SAR data, include (1) a manual photographic interpretation, (2) one- and two-dimensional spectral analyses employing FFT techniques, and (3) extraction of band-pass filtered long-period components from radar backscatter plots. It should be mentioned when utilizing SAR data such as presented in this paper that the spectral estimates presented are wave number, directional spectra of the radar return intensity. The data do not represent wave height information in a direct sense. SAR intensities (i.e., crest-to-trough modulation) have been successfully correlated to wave height, but the exact mathematical modulation transfer function (i.e., SAR gravity wave imaging mechanism) is not totally understood at the present time.

Acknowledgments. The ERIM analysis of the SAR gravity wave data was supported by the Office of Naval Research (ONR) contract N00014-76-C-1048. The technical monitor for this ONR contract is Hans Dolezalek. The field installation of the mobile wave and current monitoring system, as well as the reduction of the in situ sea truth data, was supported by The University of Michigan Rackham grant 387349.

REFERENCES

Ausherman, D. A., W. D. Hall, J. N. Latta, and J. S. Zelenka, Radar data processing and exploitation facility, paper presented at International Radar Conference, IEEE, Washington, D. C., 1975.
Brown, W. J., and L. Porcello, An introduction to synthetic aperture radar, *IEEE Spectrum, 6,* 52–66, 1968.
Feldkamp, G. B., Correction of SAR-induced distortions in SEASAT imagery, paper presented at Conference on Applications of Digital Image Processing, Soc. of Photo-Opt. Instrum. Eng., San Diego, Calif., August 1978.
Gonzalez, F. I., R. C. Beal, W. E. Brown, P. S. DeLeonibus, J. S. Sherman, J. F. R. Gower, D. Lichy, D. B. Ross, C. L. Rufenach, and R. A. Shuchman, SEASAT synthetic aperture radar: Ocean wave detection capabilities, *Science, 204,* 1418–1421, 1979.
Gower, J. F. R., and B. A. Hughes, Radar and ship observations of coastal sea surface roughness patterns in the Gulf of Georgia, paper presented at Thirteenth International Symposium on Remote Sensing of Environment, Environ. Res. Lab. of Mich., Ann Arbor, Mich., 1979.
Jenkins, A. M., and D. G. Watts, Spectral analysis and its applications, 525 pp., Holden-Day, San Francisco, Calif., 1968.
Kasischke, E. S., Extraction of gravity wave information from space-borne synthetic aperture radar data, Master's thesis, Univ. of Mich., Ann Arbor, 1980.
Kinsman, B., *Wind Waves—Their Generation and Propagation on the Ocean Surface,* 676 pp., Prentice-Hall, Englewood Cliffs, N. J., 1965.
Kozma, A., E. N. Leith, and N. G. Massey, Tilted plane optical processor, *Appl. Opt., 11,* 1766, 1972.
Larsen, L. H., An instability of packets of short gravity waves in waters of finite depth, *J. Phys. Oceanogr., 99,* 1139–1143, 1979.
Longuet-Higgins, M. S., and R. W. Stewart, Radiation stress and mass transport in gravity waves, *J. Fluid Mech., 13,* 481–504, 1962.
Longuet-Higgins, M. S., and R. W. Stewart, Radiation stresses in water waves in a physical discussion, with applications, *Deep Sea Res., 11,* 529–562, 1964.
McGoldrick, L. F., On Wilton's ripples: A special case of resonant interactions, *J. Fluid Mech., 42,* 193–200, 1970.
McGoldrick, L. F., On the rippling of small waves: A harmonic nonlinear nearly resonant interaction, *J. Fluid Mech., 52,* 725–751, 1972.
Meadows, G. A., A field investigation of the spatial and temporal

structure of longshore currents, Ph.D. dissertation, Purdue Univ., West Lafayette, Ind., 1977.
Meadows, G. A., The wind-driven component of surf zone circulation (abstract), *Eos Trans. AGU, 60*(46), 848, 1979.
Meadows, G. A., and W. L. Wood, Long-period surf zone motions, submitted to *J. Geophys. Res.*, 1982.
Meadows, G. A., E. S. Kasischke, and R. A. Shuchman, SAR observations of coastal zone conditions, paper presented at Fourteenth International Symposium on Remote Sensing of Environment, Environ. Res. Lab. of Mich., San José, Costa Rica, 1980.
Munk, W. H., Surf beats, *Eos Trans. AGU, 30,* 849–854, 1949.
Phillips, O. M., The structure of short gravity waves on the ocean surface, in *A Symposium to Explore the Potential of Spaceborne Synthetic Aperture Radar for Radio Oceanography*, Johns Hopkins Press, Baltimore, Md., 1981.
Rawson, R., F. Smith, and R. Larson, The ERIM simultaneous *X*- and *L*-band dual polarized radar, paper presented at International Radar Conference, IEEE, Washington, D. C., 1975.
Schwab, D., R. A. Shuchman, and D. Liu, Wind wave directions determined from synthetic aperture radar imagery and from a tower in Lake Michigan, *J. Geophys. Res., 86*(C3), 2059–2064, 1981.
Shuchman, R. A., and G. A. Meadows, Airborne synthetic aperture radar observations of surf zone conditions, *Geophys. Res. Lett.*, *7*(11), 857–860, 1980.
Shuchman, R. A., K. Knorr, J. C. Dwyer, A. Klooster, and A. I. Maffett, Imaging ocean waves with SAR, *ERIM Rep. 124300-2-T,* 130 pp., Environ. Res. Inst. of Mich., Ann Arbor, Mich., 1979.
Tucker, M. J., Surf beats: Sea waves of 1 to 5 minutes period, *Proc. R. Soc. London Ser. A, 207,* 565–573, 1950.
Whitham, G. B., Mass momentum and energy flux in water waves, *J. Fluid Mech., 12,* 135–147, 1962.
Wood, W. L., and G. A. Meadows, Unsteadiness in longshore currents, *Geophys. Res. Lett., 2*(11), 503–505, 1975.
Wright, J. W., A new model for sea clutter, *IEEE Trans. Antennas Propag., AP-16,* 195–223, 1968.

(Received April 21, 1981;
revised January 29, 1982;
accepted February 1, 1982.)